Autoionization from the plasmon resonance in isolated 1-cyanonaphthalene

James N. Bull,[1, 2, a)] Paola Bolognesi,[3] Cate S. Anstöter,[4] Eleanor K. Ashworth,[1] José E. Navarro Navarrete,[5] Boxing Zhu,[5] Robert Richter,[6] Nitish Pal,[6] Jacopo Chiarinelli,[3] Lorenzo Avaldi,[3] Henning Zettergren,[5] and Mark H. Stockett[5]

[1)] *School of Chemistry, Norwich Research Park, University of East Anglia, Norwich NR4 7TJ, United Kingdom*

[2)] *Centre for Photonics and Quantum Science, University of East Anglia, Norwich NR4 7TJ, United Kingdom*

[3)] *CNR-Istituto di Struttura della Materia, Area della Ricerca di Roma 1, Rome, Italy*

[4)] *Department of Chemistry, University of York, Heslington, York, YO10 5DD, United Kingdom*

[5)] *Department of Physics, Stockholm University, SE-10691 Stockholm, Sweden*

[6)] *Elettra Sincrotrone Trieste, Trieste, Italy*

Polycyclic aromatic hydrocarbons have been widely conjectured to be ubiquitous in space, as supported by the recent discovery of two isomers of cyanonaphthalene, indene, and 2-cyanoindene in the Taurus Molecular Cloud-1 using radioastronomy. Here, the photoionization dynamics of 1-cyanonaphthalene (1-CNN) are investigated using synchrotron radiation over the $h\nu = 9.0$–$19.5\,\mathrm{eV}$ range, revealing that prompt autoionization from the plasmon resonance dominates the photophysics for $h\nu = 11.5$–$16.0\,\mathrm{eV}$. Minimal photo-induced dissociation, whether originating from an excited state impulsive bond rupture or through internal conversion followed by a statistical bond cleavage process, occurs over the microsecond timescale (as limited by the experimental setup). The direct photoionization cross-section and photoelectron angular distributions are simulated using an ezDyson model combining Dyson orbitals with Coulomb wave photoejection. When considering these data in conjunction with recent radiative cooling measurements on 1-CNN$^+$, which showed that cations formed with up to 5 eV of internal energy efficiently stabilize through recurrent fluorescence, we conclude that the organic backbone of 1-CNN is resilient to photodestruction by VUV and soft XUV radiation. These dynamics may prove to be a common feature for the survival of small polycyclic aromatic hydrocarbons in space, provided that the cations have a suitable electronic structure to support recurrent fluorescence.

For more than three decades, polycyclic aromatic hydrocarbons (PAHs) have been conjectured to be abundant in space;[1–3] they are surmised to dominate mid-infrared emissions,[4–7] including the so-called aromatic infrared bands (AIBs) in UV-irradiated astrochemical environments.[6,8,9] These IR emission bands are ubiquitous in the universe, observed across many astrochemical environments, including the galactic interstellar medium, planetary nebulae, star forming regions, and other galaxies.[10,11] Only in the last few years have specific PAHs been identified in the cold, dark molecular cloud TMC-1 (Taurus Molecular Cloud-1) through comparing radioastronomy observations with spectra recorded in the laboratory.[12–14] Significantly, the observed abundances of two cyanonaphthalene isomers were six orders of magnitude higher than astrochemical modeling predicted;[12] there are similar abundance discrepancies between observations and modeling for the other identified PAHs.[13–15] Prior to these identifications, it was thought that PAHs with less than ≈50 atoms would not radiatively stabilize following ionizing interactions.[16–18]

In a step towards characterizing the dynamic processes leading to the preponderance of 1-cyanonaphthalene (1-

CNN, FIG. 1) in TMC-1, some of the current authors used the cryogenic Double ElectroStatic Ion storage Ring ExpEriment (DESIREE) facility at Stockholm University to demonstrate efficient radiative cooling of the radical cation 1-CNN$^+$ through recurrent fluorescence (RF).[23,24] RF is a relaxation mechanism associated with radiative emission from thermally populated electronic states, accessed through a process known as inverse internal conversion.[25,26] The occurrence of RF appears common in isolated PAH cations,[27–32] and maybe more active than previously thought in many PAHs because Herzberg-Teller coupling increases the intensity of the low-lying electronic transitions.[23,33] The DESIREE study demonstrated that 1-CNN$^+$ can radiatively stabilize efficiently through RF when formed with up to 5 eV worth of vibrational energy,[23] which is

a)Electronic mail: james.bull@uea.ac.uk
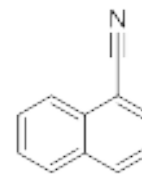
FIG. 1. Molecular structure of 1-cyanonaphthalene (1-CNN). The radical cation is denoted 1-CNN$^+$.
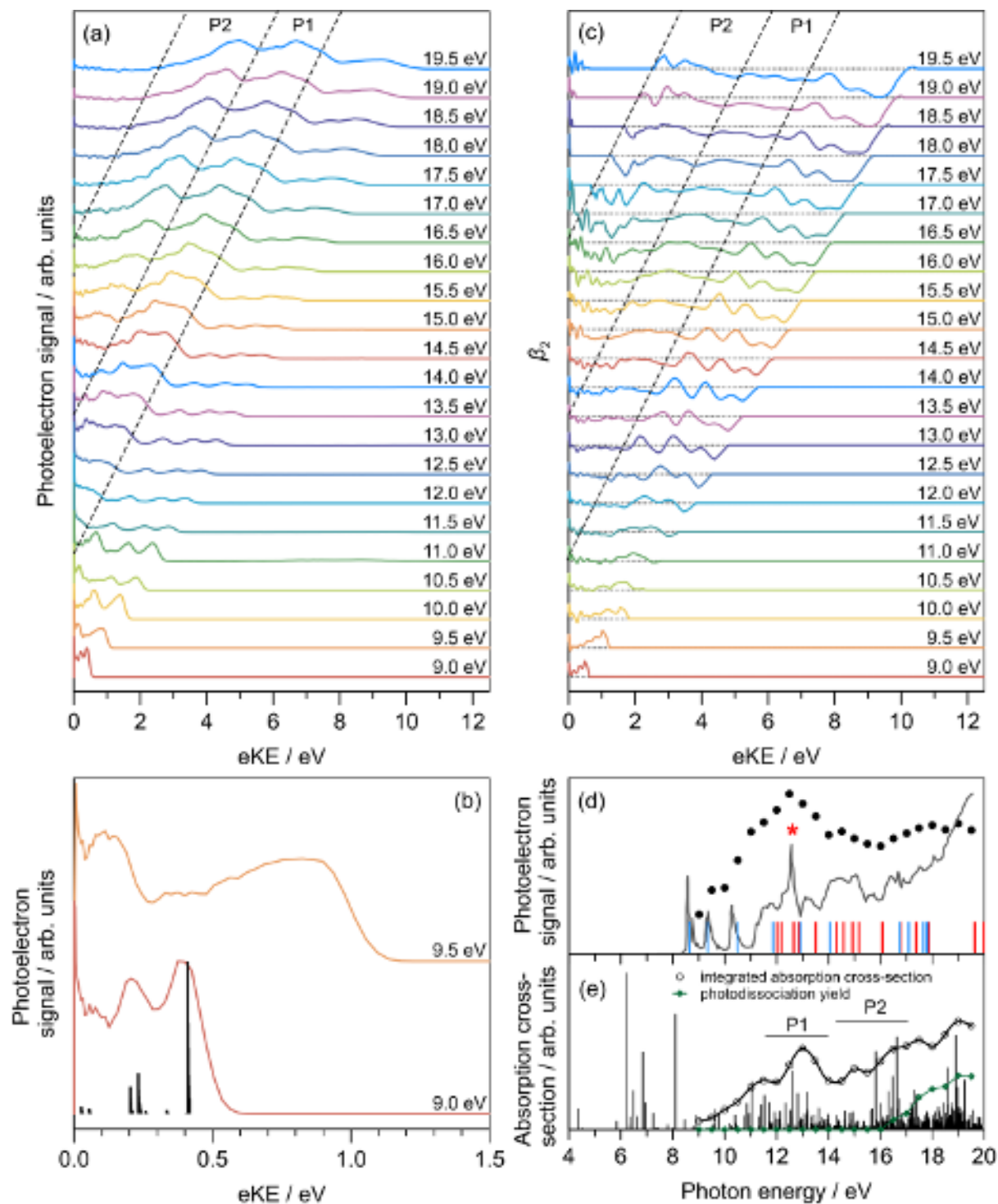
FIG. 2. Photoelectron spectroscopy of 1-CNN recorded using tunable synchrotron radiation: (a) Intensity-normalized photoelectron spectra recorded in $0.5\,\mathrm{eV}$ photon energy increments – see Supplementary Material for photoelectron spectra plotted individually. P1 and P2 refer to the two bands of the plasmon resonance (arbitrary division). (b) Expanded energy scale photoelectron spectra at $h\nu = 9.0$ and $9.5\,\mathrm{eV}$ (solid traces), including a Franck-Condon simulation[19] of the $D_1[1A'']\leftarrow S_0$ manifold (sticks). (c) β_2 angular anisotropy values with photon energy. (d) Photoionization spectrum (i.e. relative cross-section) with photon energy (black solid circles). The grey trace is a He I ($21.2\,\mathrm{eV}$) photoelectron spectrum for 1-CNN from Ref. 20, with the red asterisk indicating signal from H_2O contamination. The sticks correspond to computed vertical ionization potentials at the EOM-IP-CCSD/cc-pVTZ level of theory for ionization to A' (red) and A'' (blue) electronic states of the cation. (e) Calculated electronic transitions of 1-CNN at the df-CC2/cc-pVTZ level of theory (vertical sticks) – this method includes excitations with singles and doubles character,[21] which are those with any significant oscillator strength.[22] The amalgamation of electronic states over the $h\nu = 11$–$18\,\mathrm{eV}$ range constitutes the so-called plasmon resonance (P1 + P2). For ease of comparison with the experimental data, the integrated absorption cross-section, in $0.5\,\mathrm{eV}$ intervals, is included (open circles). The photodissociation curve from our measurements (not to scale) is included in green; photodissociaiton contributes only a few percent at $h\nu = 19.5\,\mathrm{eV}$.

$\approx 2\,\mathrm{eV}$ beyond the bond dissociation threshold ($\approx 3\,\mathrm{eV}$).[34] Because the ionization potential of 1-CNN is $\approx 8.59\,\mathrm{eV}$,[35] 1-CNN$^+$ generated through interaction with $\mathrm{H}^+ + e^-$ recombination radiation ($13.6\,\mathrm{eV}$) or Lyman-α ($10.2\,\mathrm{eV}$) should be resilient to decomposition of the organic backbone because RF cooling out-competes dissociation. However, despite the astrochemical importance of neutral 1-CNN, little is known about its detailed photoionization dynamics.

In this work, we used the CiPo beamline[36] at the Elettra-Sincrotrone Trieste laboratory (Trieste, Italy) to record photoelectron velocity-map images for 1-CNN following photoionization with $h\nu = 9.0$–$19.5\,\mathrm{eV}$ radiation (in $0.5\,\mathrm{eV}$ increments). Details of the velocity-map imaging end station and experimental arrangement are available elsewhere.[37] Briefly, $\approx 3\,\mathrm{g}$ of 1-CNN (Sigma-Aldrich, $>99\%$ purity) was loaded into a sample vessel connected to a heated (temperature controlled) nozzle ($2\,\mathrm{mm}$ diameter) with a skimmer assembly. The sample was kept at $T = 323\,\mathrm{K}$ and the nozzle at $T = 358\,\mathrm{K}$. No sample decomposition was evident. These conditions gave a working pressure in the range of high-10^{-8} to low-$10^{-7}\,\mathrm{mbar}$, on a base vacuum chamber pressure of $1 \times 10^{-8}\,\mathrm{mbar}$. Velocity-map images of the photoelectrons were accumulated in coincidence with the parent ion in order to avoid photoelectron signal originating from fragments or contaminants, such as background $\mathrm{H_2O}$. The images were processed using antialiasing and polar onion peeling algorithms to obtain photoelectron spectra and photoelectron angular distributions (PADs).[38] The velocity-to-energy conversion was calibrated using atomic photoelectron spectra of neon and xenon.[39] The $\Delta E/E$ resolution of the imaging assembly is $\approx 6\%$, and extracted PADs (as β_2 values) have uncertainties of typically ± 0.1. The photoionization spectrum was normalized with respect to photon flux at each photon energy. The photoionization spectrum in this work is often referred to as the total co-incidence photoelectron spectrum (or total electrons in co-incidence with the parent ion for photon energies after fragmentation channels become accessible). Higher-order effects in the synchrotron radiation were negligible, as evidenced from the velocity-map images.

Signal intensity in the PADs, $I(\theta)$, is described by

$$I(\theta) = \frac{\sigma}{4\pi}\left[1 + \beta_2 P_2(\cos\theta)\right], \qquad (1)$$

where θ is the polar angle between the polarization vector of the radiation and the velocity vector of the ejected photoelectron, σ is the direct photoionization cross-section for a given photon energy, and β_2 is the so-called anisotropy parameter conventionally used to quantify the degree of anisotropy.[40] For a single-photon ionization, β_2 values for the photoelectrons range between $+2$ and -1, with the limits corresponding to a $\cos^2\theta$ (parallel) and a $\sin^2\theta$ (perpendicular) distribution relative to the polarization vector, respectively, for atomic orbitals.[41] $P_2(\cos\theta)$ is a second-order Lengendre polynomial. For electron ejection from molecular orbitals, β_2 values

typically span a reduced range. A non-zero β_2 for a single-photon ionization means that electron ejection occurs more rapidly than molecular rotation (picoseconds for 1-CNN at $T \approx 300\,\mathrm{K}$). When several ionization processes produce photoelectrons with the same kinetic energy, the β_2 values reflect a sum, making their interpretation non-trivial.

Photoelectron spectra for 1-CNN are shown in FIG. 2a, with the $h\nu = 9.0$ and $9.5\,\mathrm{eV}$ spectra shown expanded in FIG. 2b. The corresponding PADs, quantified as β_2 values, are shown in FIG. 2c. The photoionization spectrum associated with formation of 1-CNN$^+$ (measured in coincidence) is given in FIG. 2d, along with a He I ($21.2\,\mathrm{eV}$) photoelectron spectrum (horizontal abscissa corresponds to electron kinetic energy) for 1-CNN from Ref. 20, and also our computed vertical ionization potentials. Computed vertical electronic transition energies of 1-CNN are shown in FIG. 2e.

The photoelectron spectra reveal several bands, most prominently appearing for $h\nu < 11.5\,\mathrm{eV}$, where the photoionization yield is maximized (FIG. 2d). The photoelectron spectrum at $h\nu = 9.0\,\mathrm{eV}$ shows vibronic structure, which has been assigned to the $\mathrm{D_1[1A'']} \leftarrow \mathrm{S_0}$ ionization with the structure associated with fundamental and combination bands involving 1430 and $1700\,\mathrm{cm}^{-1}$ in-plane stretching modes. This vibronic structure is consistent with earlier He I ($21.2\,\mathrm{eV}$) and He II ($40.8\,\mathrm{eV}$) photoelectron spectra,[20,35] and provides the ionization potential at $8.60 \pm 0.03\,\mathrm{eV}$, in agreement with the literature values of 8.59 and $8.61\,\mathrm{eV}$ (no uncertainties given). Note that He I and He II photoelectron spectra should be (predominantly) non-resonant and thus reflect only direct photoionization processes. Two further photoelectron peaks corresponding to binding energies of $\approx 9.35\,\mathrm{eV}$ ($9.35\,\mathrm{eV}$ in Ref. 20) and $\approx 10.28\,\mathrm{eV}$ ($10.31\,\mathrm{eV}$ in Ref. 20) are associated with the second ($\mathrm{D_1[2A'']} \leftarrow \mathrm{S_0}$) and third ($\mathrm{D_2[3A'']} \leftarrow \mathrm{S_0}$) lowest ionization transitions, respectively, and are similarly consistent with the He I photoelectron spectrum. As described below, β_2 values associated with the first two lowest ionization transitions are reproduced using a model combining Dyson orbitals and Coulomb wave electron ejection.

For $11 \leq h\nu \leq 18\,\mathrm{eV}$, our excited state calculations on 1-CNN indicate there are ≈ 20 ionization transitions, resulting in complex photoelectron spectra and β_2 values. Furthermore, this photon energy spans the so-called plasmon resonance. The term plasmon resonance describes a fascinating property of isolated PAHs, which manifests as a broad autoionizing resonance in the $h\nu = 14$–$18\,\mathrm{eV}$ range (closer to $h\nu = 11.5$–$17\,\mathrm{eV}$ in this work) in electronic absorption spectra, photo-ion yield curves, and electron energy loss spectra.[42,43] This feature has been interpreted as arising from a high density or 'pile up' of indistinguishable excitations to π^* and σ^* states whose excitation cross-section is augmented by electron correlation effects.[43,44] Because these states, which are technically shape and Feschbach

resonances, are all strongly overlapping in excitation energy and are coupled to some degree, they are treated as a collective. By analogy to similar electronic structure in fullerenes, graphene, and three-dimensional materials, this feature is commonly referred to as the plasmon resonance in isolated PAHs.[45] Although the plasmon resonance is situated in the detachment continuum and is open to spontaneous electron ejection through vibrational autoionization,[46] some combination of centrifugal, polarization, and exchange forces lead to a temporary binding interaction with valence-localized character.[47] The plasmon resonance for 1-CNN was modeled (FIG. 2e) by integrating the calculated oscillator strengths ($\approx$600 states up to $20\,\mathrm{eV}$) and assuming $0.5\,\mathrm{eV}$ absorption profiles (i.e. $0.5\,\mathrm{eV}$ full-width half-maximum, FWHM) for each transition, which is assumed limited by Franck-Condon profiles rather than lifetime effects. We note that the feature is dominated by $\pi - \pi^*$ transitions since they typically have oscillator strengths an order of magnitude or more larger than transitions to σ^* states. Due to the number of excited states, our simple integration model of the plasmon resonance does not consider vibronic structure of the individual transitions. However, we note that the model does satisfactorily account for the peak in the photoionization spectrum at $\approx$13 eV (FIG. 2e).

To help understand the direct photoionization (i.e. non-resonant) processes active for 1-CNN, and to provide an interpretation of the β_2 values, we modeled both parameters using the ezDyson 4.0 program[48] with input Dyson orbitals computed at the EOM-IP-CCSD/cc-pVDZ level of theory in Q-Chem 6.0.[49] The choice of methodology was guided by earlier benchmarking efforts.[50] The Dyson spin-orbitals for ionization of an electron with spatial coordinate x_1 are defined as overlaps between initial (Ψ_i) N-electron states and final states (Ψ_f) with $N - 1$ electrons:[51]

$$\psi_D(x_1) = \sqrt{N} \int \Psi_f^*(x_2, x_3, ..., x_N) \times \Psi_i(x_1, x_2, x_3, ..., x_N) dx_2 dx_3 ... dx_N. \quad (2)$$

Computed direct photoionization cross-sections to the accessible A$''$ (π-like ejection) and A$'$ (σ-like ejection) states of the neutral are shown in FIG. 3a. Corresponding Dyson orbitals for the first four ionized states of each symmetry class are shown in FIG. 3b. The sum of the state-specific direct photoionization (DPI) cross-sections is shown in FIG. 3c, and is unable to account for either the shape of photoionization spectrum nor the broad peak at $\approx$12.5 eV. On the other hand, our plasmon model (FIG. 3c, orange), combining the DPI model and the absorption cross-section curve (FIG. 2e), reproduces the shape and the peak feature at $\approx$12.5 eV in the photoionization spectrum. Our model is simplistic – it assumes that individual electronic transitions in the plasmon resonance all have a $0.5\,\mathrm{eV}$ width absorption profile and all excitations lead to vibrational

autoionization.[46] The latter of these assumptions is consistent with the fact that photodissociation was observed only for $h\nu$ >16 eV (FIG. 2c), although dissociation signal level in the experiment was only a few percent compared with the parent photoion signal. The main photofragments corresponded to loss of HCN, H, and C_2H_2, consistent with observations from a collision-induced dissociation study.[34] Ultimately, we conclude that excitation to the plasmon resonance followed by autoionization is more probable than direct photoionization, and that the probability for dissociation, directly or indirectly (i.e. after internal conversion) following excitation of the plasmon resonance, is very low.

Comparing modeled β_2 values with experiment is straight-forward for the first few ionization potentials leading to A$''$ states (FIG. 3d and Supplementary Material) because the spectral bands in the photoelectron spectra are well separated, with minimal contamination from autoionizing states. The consistency between theory and experiment gives confidence that the PADs for direct photoionization can be modeled adequately. On the other hand, the large number of ionization thresholds and excited electronic states of the neutral over the $h\nu = 11$–18 eV range mean that the measured β_2 values result from the sum (incoherent superposition) of many direct photoionization and prompt autoionization processes. Broadly speaking, simulated β_2 values for ionization to A$'$ states are positive, while those for ionization to A$''$ states are negative (see Supplementary Material). Experimental β_2 values, averaged over the P1 and P2 features (as indicated in FIG. 2a), are shown in FIG. 3e and are predominately negative. This trend correlates with the main fraction of photoelectrons arising from prompt autoionization of $\pi - \pi^*$ states, where prompt implies that electron ejection occurs more rapidly than molecular rotation; such a process resembles direct photodetachment to an A$''$ state. We note that the P2 feature shows quite negative β_2 values for $h\nu = 15$–18 eV (FIG. 3e), consistent with several strong $\pi - \pi^*$ transitions followed by prompt autoionization. In summary, trends in simulated and experimental β_2 values are consistent with the interpretation that autoionization from the plasmon resonance is the dominant electron ejection process for 1-CNN over the $h\nu = 11.5$–17 eV range. In our above interpretation, the division of the plasmon resonance between P1 and P2 regions is somewhat arbitrary, but was guided by the double-peaked feature in the photoelectron spectra (FIG. 2a). For larger PAHs with more excitations contributing to the plasmon resonance and further direct photoionization thresholds, this structure will likely disappear.

This work has considered the photoionization and autoionization dynamics of 1-CNN, a molecule which has been identified through radioastronomy in the cold, dark molecular cloud TMC-1. The present study indicates that, when subjected to VUV and soft XUV radiation, such as $13.6\,\mathrm{eV}$ photons generated through H$^+$ + e^-
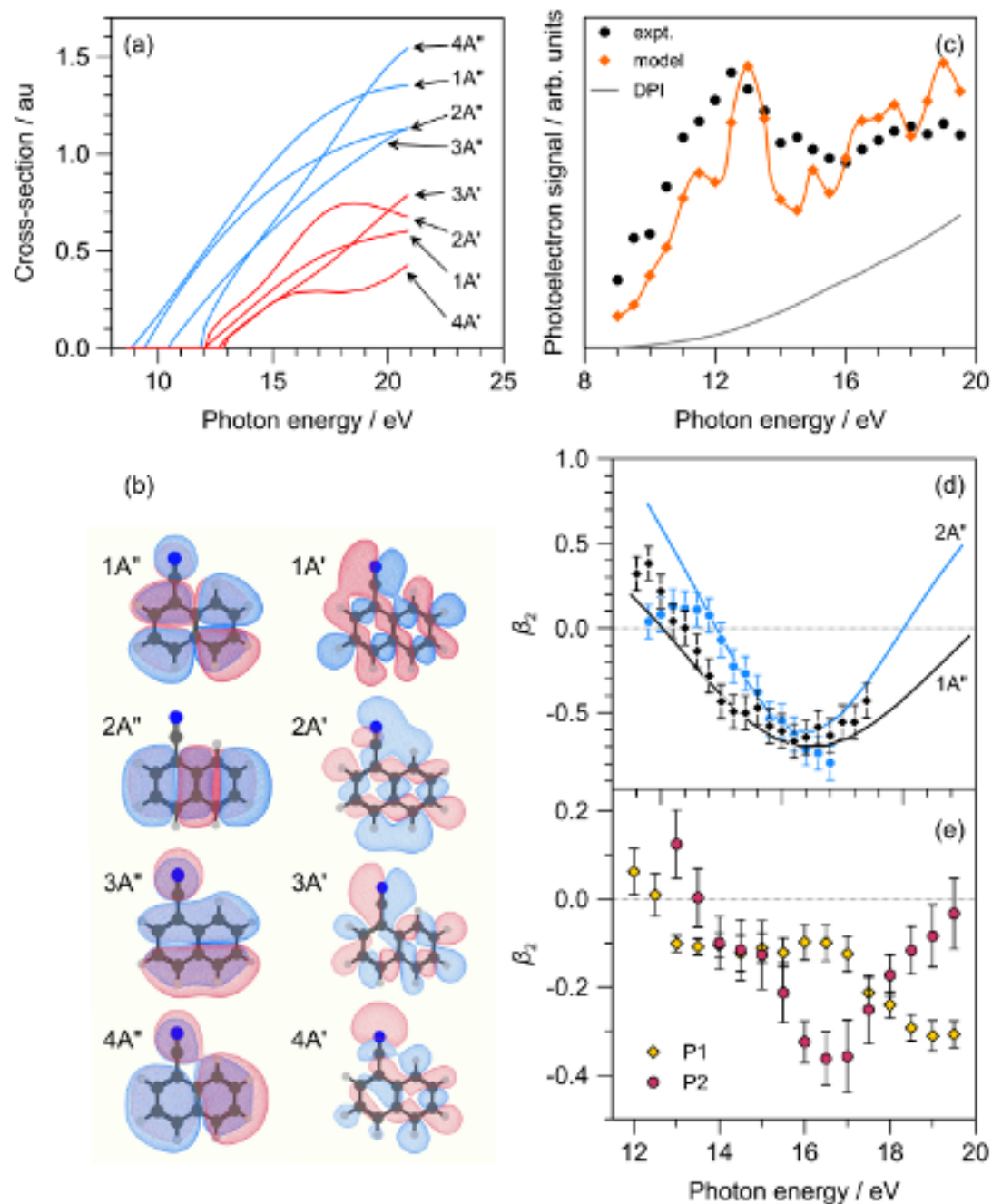
FIG. 3. Dyson orbital simulations for 1-CNN: (a) State-specific direct photoionization cross-sections (atomic units) for formation of the first four A″-symmetry states (blue traces) and A′-symmetry states (red traces) of the cation. Cross-sections and Dyson orbitals for the other ionized states are given in the Supplementary Material. (b) Illustrations of the Dyson orbitals associated with the first four A″ (π-electron ejection) and A′ (σ-electron ejection) states of the cation. Further Dyson orbitals are shown in the Supplementary Material. (c) Total direct photoionization (DPI) cross-section (grey solid trace), obtained by summing state-specific cross-sections in FIG. 2a, and modeled ionization profile (orange) combining the DPI and autoionization models, compared with the measured photoionization spectrum (black) from FIG. 2d. (d) Simulated (solid curves) and experimental β_2 values for direct photoionization to the 1A″ and 2A″ states (see Supplementary Material). (e) β_2 values averaged over the P1 (yellow diamonds) and P2 (red circles) bands of the plasmon resonance. These values are predominately negative, consistent with autoionization from $\pi - \pi^*$ transitions rather than direct photoionization to an array of A′ states. Note the differing vertical abscissa scales in (d) and (e), and that β_2 values in (e) are small compared with the limiting β_2 values (+2 and −1).

recombination or the Lyman-α line at $10.2\,\text{eV}$,[52] the molecule is most likely to be photoexcited to the plasmon resonance, which promptly autoionizes. These hydrogen emission lines correspond to the most abundant photon energies in many astrochemical environments.[52] The probability for photodissociation of 1-CNN, either on an excited state or after internal conversion to the ground electronic state, is low over the microsecond timescale. This conclusion is consistent with the fact that photodissociation signal in this work, albeit weak, is present for $h\nu > 16\,\text{eV}$, although we note that the observation of dissociation could be restricted by the short time between ionization and ion detection ($\approx 1\,\mu\text{s}$), i.e. the experimental window. We acknowledge that some fraction of slower, statistical dissociation (and potentially isomerization) may occur, although this is likely small based on our 1-CNN$^+$ DESIREE experiments where we monitored quenching of neutral production (through dissociation) by RF.[23,24] Combining the results from this work with those from our recent DESIREE studies on 1-CNN$^+$,[23,24] which showed that cations formed with up to 5 eV of internal vibrational energy (or a minimum photon energy of $13.6\,\text{eV}$ when ionizing neutral 1-CNN) are able to radiatively stabilize through RF without dissociating,[23] leads to the sequence of dynamics summarised in FIG. 4. The astrophysical significance of these dynamics is that 1-CNN is unlikely to exist as neutral molecules in UV-dominated regions of space, such as photodissociation regions (PDRs);[53] rather, the organic framework will be present as 1-CNN$^+$. In dark molecular clouds such as TMC-1, the 1-CNN vs 1-CNN$^+$ charge balance will be determined by the competition between photoionization (by VUV photons and cosmic rays) and electron-ion/ion-ion recombination.[52,54]

We propose that similar autoionization and radiative cooling dynamics are a key ingredient for the VUV and soft XUV photoresilience of other PAHs that can survive in space. The above photoionization and radiative cooling dynamics challenge the conventional wisdom[16–18] that energized interstellar PAHs radiatively cool only through infrared emission, which occurs substantially more slowly and less efficiently than RF cooling,[30,59–62] and, consequently, that only PAHs with more than ≈ 50 atoms can radiatively stabilize.[2] It is clear that further experiments on the radiative cooling and photoionization dynamics of PAHs that are thought to exist in space, including the known PAHs indene and 2-cyanoindene,[13,14] are needed to establish 'rules of thumb' for determining interstellar PAH propensity.

Finally, we note that recent XUV-IR experiments have sought to investigate ultrafast relaxation dynamics of PAH cations formed their so-called correlation band (CB,[63] an amalgamation of bound, ionized states situated below the lowest double ionization threshold).[64,65] In contrast, the plasmon resonance discussed in this work is due to the amalgamation of excited states situated above the lowest ionization
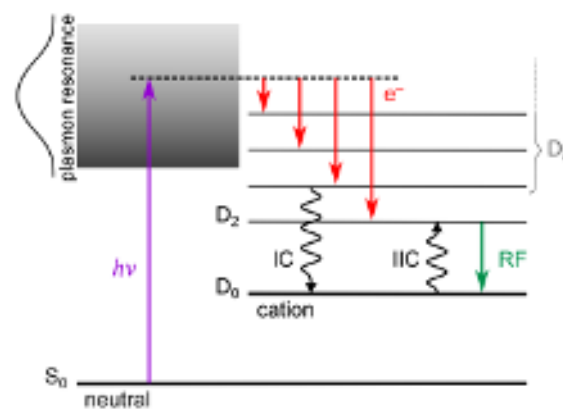
FIG. 4. Summary of the photo-induced dynamics of 1-CNN resulting in photoresilence of the organic backbone in space. Following absorption of a photon ($h\nu$) exciting the plasmon resonance, autoionization[46] produces various electronic states of 1-CNN$^+$ (D_n). Ensuing internal conversion (IC) forms the ground electronic state of 1-CNN$^+$. In turn, after statistical internal energy redistribution, inverse internal conversion (IIC) may populate the D_2 electronic state of the cation, which may radiatively relax through recurrent fluorescence (RF).[23] The cross-section for autoionization to directly populate to the D_2 state is low compared with the summed cross-section to other cationic states. Experiments on PAH cations have characterized that IC typically occurs on the picosecond timescale.[55–58]

threshold of the neutral molecule. For naphthalene, the XUV-IR study used $\approx 23\,\text{eV}$ photons to generate the cation; this photon energy is situated well above the expected plasmon resonance[45] for (neutral) naphthalene and at an energy where the total direct photoionization cross-section should exceed the excitation cross-section. In future experiments, it would be interesting to apply time-resolved strategies to 1-CNN, or similar molecules, with the pump pulse tuned to excite the plasmon resonance.

SUPPLEMENTARY MATERIAL

The Supplementary Material contains details on: expanded plots of all photoelectron spectra and β_2 values, illustrations of Dyson orbitals, all modeled state-specific photoionization cross-sections for the A'- and A''-symmetry states, β_2 values for the 1A'' and 2A'' ionized states modeled with different basis sets, modeled state-specific direct photoionization cross-sections and β_2 values for each ionized state.

DATA AVAILABILITY

The data that support the findings of this study are available from the authors upon reasonable request.

ACKNOWLEDGMENTS

AUTHOR CONTRIBUTIONS

This work was based on a beamtime application prepared by MHS and JNB. Analysis of experimental data was performed by EKA, JENN, BZ, and JNB. PB, JENN, BZ, RR, NP, JC, and LA participated in experimental data acquisition. Electronic structure calculations were performed by CSA, EKA, and JNB. The manuscript was prepared by JNB with assistance from EKA, and was discussed by all authors.

CONFLICTS OF INTEREST

The authors have no conflicts to disclose.

REFERENCES

[1] W. W. Duley and D. A. Williams, Mon. Not. Royal Astron. Soc. **196**, 269 (1981).

[2] L. J. Allamandola, G. G. M. Tielens, and J. R. Barker, Astrophys. J. Supp. Ser. **71**, 733 (1989).

[3] A. G. G. M. Tielens, Rev. Mod. Phys. **85**, 1021 (2013).

[4] A. G. G. M. Tielens, Ann. Rev. Astron. Astrophys. **46**, 289 (2008).

[5] S. Kwok and Y. Zhang, Nature **479**, 80 (2011).

[6] A. Li, Nat. Astron. **4**, 339 (2020).

[7] S. Kwok, Astrophys. Space Sci. **367**, 16 (2022).

[8] G. Lagache, H. Dole, J.-L. Puget, P. G. Pérez-González, E. L. Floc'h, G. H. Rieke, C. Papovich, E. Egami, A. Alonso-Herrero, C. W. Engelbracht, K. D. Gordon, K. A. Misselt, and J. E. Morrison, Astrophys. J. Supp. Ser. **154**, 112 (2004).

[9] J. D. T. Smith, B. T. Draine, D. A. Dale, J. Moustakas, R. C. K. Jr., G. Helou, L. Armus, H. Roussel, K. Sheth, G. J. Bendo, B. A. Buckalew, D. Calzetti, C. W. Engelbracht, K. D. Gordon, D. J. Hollenbach, A. Li, S. Malhotra, E. J. Murphy, and F. Walter, Astrophys. J. **656**, 770 (2007).

[10] E. Peeters, H. W. W. Spoon, and A. G. G. M. Tielens, Astrophys. J. **613**, 986 (2004).

[11] O. Berné, C. Joblin, A. Fuente, and F. Ménard, Astron. Astrophys. **495**, 827 (2009).

[12] B. A. McGuire, R. A. Loomis, A. M. Burkhardt, K. L. K. Lee, C. N. Shingledecker, S. B. Charnley, I. R. Cooke, M. A. Cordiner, E. Herbst, S. Kalenskii, M. A. Siebert, E. R. Willis, C. Xue, A. J. Remijan, and M. C. McCarthy, Science **371**, 1265 (2021).

[13] A. M. Burkhardt, K. L. K. Lee, P. B. Changala, C. N. Shingledecker, I. R. Cooke, R. A. Loomis, H. Wei, S. B. Charnley, E. Herbst, M. C. McCarthy, and B. A. McGuire, Astrophys. J. Lett. **913**, L18 (2021).

[14] M. L. Sita, P. B. Changala, C. Xue, A. M. Burkhardt, C. N. Shingledecker, K. L. K. Lee, R. A. Loomis, E. Momjian, M. A. Siebert, D. Gupta, E. Herbst, A. J. Remijan, M. C. McCarthy, I. R. Cooke, and B. A. McGuire, Astrophys. J. Lett. **938**, L12 (2022).

[15] J. Cernicharo, M. Agúndez, C. Cabezas, B. Tercero, N. Marcelino, J. R. Pardo, and P. de Vicente, Astron. Astrophys. **649**, L15 (2021).

[16] M. Rapacioli, F. Calvo, C. Joblin, P. Parneix, D. Toublanc, and F. Spiegelman, Astron. Astrophys. **460**, 519 (2006).

[17] J. Montillaud, C. Joblin, and D. Toublanc, Astron. Astrophys. **552**, A15 (2013).

[18] M. Chabot, K. Béroff, E. Dartois, T. Pino, and M. Godard, Astrophys. J. **888**, 17 (2019).

[19] F. Santoro, A. Lami, R. Improta, J. Bloino, and V. Barone, J. Chem. Phys. **128**, 224311 (2008).

[20] C. Utsunomiya, T. Kobayashi, and S. Nagakura, Bull. Chem. Soc. Japan **48**, 1852 (1975).

[21] D. Mester, P. R. Nagy, and M. Kállay, J. Chem. Phys. **146**, 194102 (2017).

[22] R. Izsák, WIREs Comp. Mol. Sci. **10** (2019).

[23] M. H. Stockett, J. N. Bull, H. Cederquist, S. Indrajith, M. Ji, J. E. Navarro Navarrete, H. T. Schmidt, H. Zettergren, and B. Zhu, Nat. Comm. **14**, 395 (2023).

[24] J. E. Navarro Navarrete, J. N. Bull, H. Cederquist, S.Indrajith, M. Ji, H. T. Schmidt, H. Zettergren, B. Zhu, and M. H. Stockett, Faraday Discuss. 10.1039/d3fd00005b (2023).

[25] A. Nitzan and J. Jortner, J. Chem. Phys. **71**, 3524 (1979).

[26] A. Léger, P. Boissel, and L. d'Hendecourt, Phys. Rev. Lett. **60**, 921 (1988).

[27] M. Saito, H. Kubota, K. Yamasa, K. Suzuki, T. Majima, and H. Tsuchida, Phys. Rev. A **102**, 012820 (2020).

[28] J. Bernard, L. Chen, R. Brédy, M. Ji, C. Ortéga, J. Matsumoto, and S. Martin, Nucl. Instrum. Meth. Phys. Res. B **408**, 21 (2017).

[29] M. Ji, J. Bernard, L. Chen, R. Brédy, C. Ortéga, C. Joblin, A. Cassimi, and S. Martin, J. Chem. Phys. **146**, 044301 (2017).

[30] M. H. Stockett, J. N. Bull, J. T. Buntine, E. Carrascosa, M. Ji, N. Kono, H. T. Schmidt, and H. Zettergren, J. Chem. Phys. **153**, 154303 (2020).

[31] J. W. L. Lee, M. H. Stockett, E. K. Ashworth, J. E. Navarro Navarrete, E. Gougoula, D. Garg, M.-C. Ji, B. Zhu, S. Indrajith, H. Zettergren, H. T. Schmidt, and J. N. Bull, J. Chem. Phys. **158**, 174305 (2023).

[32] U. Jacovella, A. Giuliani, C. S. Hansen, A. J. Trevitt, L. Nahon, G. Malloci, and G. Mulas, Astron. Astrophys. **670**, A181 (2023).

[33] G. J. Small, J. Chem. Phys. **54**, 3300 (1971).

[34] B. J. West, L. Lesniak, and P. M. Mayer, J. Phys. Chem. A **123**, 3569 (2019).

[35] L. Klasinc, B. Kovač, and H. Gusten, Pure Appl. Chem. **55**, 289 (1983).

[36] A. Derossi, F. Lama, M. Piacentini, T. Prosperi, and N. Zema, Rev. Sci. Instrum. **66**, 1718 (1995).

[37] P. O'Keeffe, P. Bolognesi, M. Coreno, A. Moise, R. Richter, G. Cautero, L. Stebel, R. Sergo, L. Pravica, Y. Ovcharenko, and L. Avaldi, Rev. Sci. Instrum. **82**, 033109 (2011).

[38] G. M. Roberts, J. L. Nixon, J. Lecointre, E. Wrede, and J. R. R. Verlet, Rev. Sci. Instrum. **80**, 053104 (2009).

[39] P. O'Keeffe, P. Bolognesi, R. Richter, A. Moise, Y. Ovcharenko, G. C. King, and L. Avaldi, Phys. Rev. A **84**, 025404 (2011).

[40] J. Cooper and R. N. Zare, J. Chem. Phys. **48**, 942 (1968).

[41] R. N. Zare, Mol. Photochem. **4**, 1 (1972).

[42] Y. Ling and C. Lifshitz, Chem. Phys. Lett. **257**, 587 (1996).

[43] H. W. Jochims, E. Ruhl, H. Baumgartel, S. Tobita, and S. Leach, Int. J. Mass Spectrom. Ion Processes **167-168**, 35 (1997).

[44] H. Gutfreund and W. A. Little, J. Chem. Phys. **50**, 4478 (1969).

[45] P. M. Mishra, L. Avaldi, P. Bolognesi, K. C. Prince, R. Richter, and U. R. Kadhane, J. Phys. Chem. A **118**, 3128 (2014).

[46] S. Pratt, Annu. Rev. Phys. Chem. **56**, 281 (2005).

[47] J. Simons, in *Resonances* (American Chemical Society, 1984) pp. 3–16.

[48] S. Gozem and A. I. Krylov, *EzDyson*, Tech. Rep. (2016).

[49] E. Epifanovsky, A. T. B. Gilbert, X. Feng, J. Lee, Y. Mao, N. Mardirossian, P. Pokhilko, A. F. White, M. P. Coons, A. L. Dempwolff, Z. Gan, D. Hait, P. R. Horn, L. D. Jacobson, I. Kaliman, J. Kussmann, A. W. Lange, K. U. Lao, D. S. Levine, J. Liu, S. C. McKenzie, A. F. Morrison, K. D. Nanda, F. Plasser, D. R. Rehn, M. L. Vidal, Z.-Q. You, Y. Zhu, B. Alam, B. J. Albrecht, A. Aldossary, E. Alguire, J. H. Andersen, V. Athavale, D. Barton, K. Begam, A. Behn, N. Bellonzi, Y. A. Bernard, E. J. Berquist, H. G. A. Burton, A. Carreras, K. Carter-Fenk, R. Chakraborty, A. D. Chien, K. D. Closser, V. Cofer-Shabica, S. Dasgupta, M. de Wergifosse, J. Deng, M. Diedenhofen, H. Do, S. Ehlert, P.-T. Fang, S. Fatehi, Q. Feng, T. Friedhoff, J. Gayvert, Q. Ge, G. Gidofalvi, M. Goldey, J. Gomes, C. E. González-Espinoza, S. Gulania, A. O. Gunina, M. W. D. Hanson-Heine, P. H. P. Harbach, A. Hauser, M. F. Herbst, M. Hernández Vera, M. Hodecker, Z. C. Holden, S. Houck, X. Huang, K. Hui, B. C. Huynh, M. Ivanov, Á. Jász, H. Ji, H. Jiang, B. Kaduk, S. Kähler, K. Khistyaev, J. Kim, G. Kis, P. Klunzinger, Z. Koczor-Benda, J. H. Koh, D. Kosenkov, L. Koulias, T. Kowalczyk, C. M. Krauter, K. Kue, A. Kunitsa, T. Kus, I. Ladjánszki, A. Landau, K. V. Lawler, D. Lefrancois, S. Lehtola, R. R. Li, Y.-P. Li, J. Liang, M. Liebenthal, H.-H. Lin, Y.-S. Lin, F. Liu, K.-Y. Liu, M. Loipersberger, A. Luenser, A. Manjanath, P. Manohar, E. Mansoor, S. F. Manzer, S.-P. Mao, A. V. Marenich, T. Markovich, S. Mason, S. A. Maurer, P. F. McLaughlin, M. F. S. J. Menger, J.-M. Mewes, S. A. Mewes, P. Morgante, J. W. Mullinax, K. J. Oosterbaan, G. Paran, A. C. Paul, S. K. Paul, F. Pavošević, Z. Pei, S. Prager, E. I. Proynov, Á. Rák, E. Ramos-Cordoba, B. Rana, A. E. Rask, A. Rettig, R. M. Richard, F. Rob, E. Rossomme, T. Scheele, M. Scheurer, M. Schneider, N. Sergueev, S. M. Sharada, W. Skomorowski, D. W. Small, C. J. Stein, Y.-C. Su, E. J. Sundstrom, Z. Tao, J. Thirman, G. J. Tornai, T. Tsuchimochi, N. M. Tubman, S. P. Veccham, O. Vydrov, J. Wenzel, J. Witte, A. Yamada, K. Yao, S. Yeganeh, S. R. Yost, A. Zech, I. Y. Zhang, X. Zhang, Y. Zhang, D. Zuev, A. Aspuru-Guzik, A. T. Bell, N. A. Besley, K. B. Bravaya, B. R. Brooks, D. Casanova, J.-D. Chai, S. Coriani, C. J. Cramer, G. Cserey, A. E. DePrince III, R. A. DiStasio Jr., A. Dreuw, B. D. Dunietz, T. R. Furlani, W. A. Goddard III, S. Hammes-Schiffer, T. Head-Gordon, W. J. Hehre, C.-P. Hsu, T.-C. Jagau, Y. Jung, A. Klamt, J. Kong, D. S. Lambrecht, W. Liang, N. J. Mayhall, C. W. McCurdy, J. B. Neaton, C. Ochsenfeld, J. A. Parkhill, R. Peverati, V. A. Rassolov, Y. Shao, L. V. Slipchenko, T. Stauch, R. P. Steele, J. E. Subotnik, A. J. W. Thom, A. Tkatchenko, D. G. Truhlar, T. Van Voorhis, T. A. Wesolowski, K. B. Whaley, H. L. Woodcock III, P. M. Zimmerman, S. Faraji, P. M. W. Gill, M. Head-Gordon, J. M. Herbert, and A. I. Krylov, J. Chem. Phys. **155**, 084801 (2021).

[50] C. S. Anstöter and J. R. R. Verlet, J. Phys. Chem. A **125**, 4888 (2021).

[51] J. V. Ortiz, J. Chem. Phys. **153**, 070902 (2020).

[52] K. I. Öberg, Chem. Rev. **116**, 9631 (2016).

[53] E. L. O. Bakes and A. G. G. M. Tielens, Astrophys. J. **499**, 258 (1998).

[54] S. Lepp and A. Dalgarno, Astrophys. J. **324**, 553 (1988).

[55] W. Cui, B. Hadas, B. Cao, and C. Lifshitz, J. Phys. Chem. A **104**, 6339 (2000).

[56] L. Zhao, R. Lian, I. A. Shkrob, R. A. Crowell, S. Pommeret, E. L. Chronister, A. D. Liu, and A. D. Trifunac, J. Phys. Chem. A **108**, 25 (2003).

[57] G. Reitsma, J. Hummert, J. Dura, V. Loriot, M. J. J. Vrakking, F. Lépine, and O. Kornilov, J. Phys. Chem. A **123**, 3068 (2019).

[58] J. W. L. Lee, D. S. Tikhonov, P. Chopra, S. Maclot, A. L. Steber, S. Gruet, F. Allum, R. Boll, X. Cheng, S. Düsterer, B. Erk, D. Garg, L. He, D. Heathcote, M. Johny, M. M. Kazemi, H. Köckert, J. Lahl, A. K. Lemmens, D. Loru, R. Mason, E. Müller, T. Mullins, P. Olshin, C. Passow, J. Peschel, D. Ramm, D. Rompotis, N. Schirmel, S. Trippel, J. Wiese, F. Ziaee, S. Bari, M. Burt, J. Küpper, A. M. Rijs, D. Rolles, S. Techert, P. Eng-Johnsson, M. Brouard, C. Vallance, B. Manschwetus, and M. Schnell, Nat. Commun. **12**, 6107 (2021).

[59] J. N. Bull, M. S. Scholz, E. Carrascosa, M. K. Kristiansson, G. Eklund, N. Punnakayathil, N. de Ruette, H. Zettergren, H. T. Schmidt, H. Cederquist, and M. H. Stockett, J. Chem. Phys. **151**, 114304 (2019).

[60] B. Zhu, J. N. Bull, M. Ji, H. Zettergren, and M. H. Stockett, J. Chem. Phys. **157**, 044303 (2022).

[61] B. Zhu, J. N. Bull, J. E. N. Navarrete, A. F. Schmidt-May, H. Cederquist, H. T. Schmidt, H. Zettergren, and M. H. Stockett, J. Chem. Phys. **157**, 174308 (2022).

[62] O. Lacinbala, F. Calvo, C. Dubosq, C. Falvo, P. Parneix, M. Rapacioli, A. Simon, and T. Pino, J. Chem. Phys. **156**, 144305 (2022).

[63] L. S. Cederbaum, W. Domcke, J. Schirmer, and W. V. Niessen, in *Adv. Chem. Phys.* (John Wiley & Sons, Inc., 2007) pp. 115–159.

[64] M. Hervé, V. Despré, P. C. Nash, V. Loriot, A. Boyer, A. Scognamiglio, G. Karras, R. Brédy, E. Constant, A. G. G. M. Tielens, A. I. Kuleff, and F. Lépine, Nat. Phys. **17**, 327 (2020).

[65] A. Boyer, M. Hervé, V. Despré, P. C. Nash, V. Loriot, A. Marciniak, A. Tielens, A. Kuleff, and F. Lépine, Phys. Rev. X **11**, 041012 (2021).